Drivers of biases in the CMIP6 extratropical storm tracks. Part II: Southern Hemisphere

Article

Accepted Version

Priestley, M. D. K., Ackerley, D., Catto, J. L. and Hodges, K. I. (2021) Drivers of biases in the CMIP6 extratropical storm tracks. Part II: Southern Hemisphere. Journal of Climate, 36 (5). pp. 1469-1486. ISSN 1520-0442 doi: https://doi.org/10.1175/JCLI-D-20-0977.1 Available at https://centaur.reading.ac.uk/99467/

To link to this article DOI: http://dx.doi.org/10.1175/JCLI-D-20-0977.1

Publisher: American Meteorological Society

Drivers of biases in the CMIP6 extratropical storm tracks. Part 2: Southern Hemisphere

Matthew D. K. Priestley[a] Duncan Ackerley[b] , Jennifer L. Catto[a] , Kevin I. Hodges[c,d]

[a] *College of Engineering, Mathematics and Physical Sciences, University of Exeter, Exeter, UK*

[b] *Met Office, Exeter, UK*

[c] *Department of Meteorology, University of Reading, Reading, UK*

[d] *NCAS, Department of Meteorology, University of Reading, Reading, UK*

Corresponding author: M. Priestley, m.priestley@exeter.ac.uk

ABSTRACT: The Southern Hemisphere storm tracks are commonly simulated too far equatorward in climate models for the historical period. In the latest generation of climate models from the 6th phase of the coupled model intercomparison project (CMIP6), the equatorward bias that was present in CMIP5 models still persists, although is reduced considerably. A further reduction of the equatorward bias is found in atmosphere-only simulations. Using diagnostic large-scale fields we propose that an increase in the midlatitude temperature gradients contributes to the reduced equatorward bias in CMIP6 and AMIP6 models, reducing the biases relative to ERA5. These changes increase baroclinicity in the atmosphere, and are associated with a storm track that is situated further poleward. In CMIP6 models, the poleward shift of the storm tracks is associated with an amelioration of cold midlatitude SST biases in CMIP5 and not through a reduction of the long-standing warm Southern Ocean SST bias. We propose that increases in midlatitude temperature gradients in the atmosphere and ocean are connected to changes in the cloud-radiative effect. Persistent track density biases to the south of Australia are shown to be connected to an apparent standing wave pattern originating in the tropics, which modifies the split jet structure near Australia and subsequently the paths of cyclones.

1. Introduction

Coupled climate models are the most sophisticated tools available for assessing potential changes to the climate in the coming century. The latest generation of models, part of the 6th phase of the coupled model intercomparison project (CMIP6; Eyring et al. 2016), represent the most recent scientific and computational advancements to help with this scientific goal. In order to assess future projections, models with a good fidelity in reproducing historical climate variability are required. However, climate models have been marred with considerable biases in relation to historical variability (e.g. Wang et al. 2014; Menary et al. 2015; Flato et al. 2013) and an understanding of the origins of these biases is required in order to determine deficiencies in, and future directions for, model development. In this study the drivers of biases in the Southern Hemisphere (SH) storm tracks are investigated. This study serves as a follow up to Priestley et al. (2020) and an accompaniment to the authors' investigation into drivers of Northern Hemisphere storm track biases (Priestley et al. 2022).

Midlatitude cyclones, and the overall storm tracks, are vital components of the Earth's climate system as they act to transfer heat and momentum polewards (Kaspi and Schneider 2013). They are also responsible for considerable amounts of midlatitude precipitation and extreme winds (e.g. Hawcroft et al. 2012; Dowdy and Catto 2017; Clark and Gray 2018). In previous generations of coupled climate models (e.g. CMIP3 and CMIP5; Meehl et al. 2007; Taylor et al. 2012), the storm track, and the general SH midlatitude circulation has tended to feature significant biases. These biases have mainly been apparent as an equatorward bias of the midlatitude circulation (Kidston and Gerber 2010; Chang et al. 2012, 2013), a zonal bias of the storm track in winter (Lee 2015), and also an underestimation of cyclone intensity (Chang et al. 2013).

In the CMIP6 models, the latitude of the SH storm track, and also the peak intensity of cyclones, is much improved and closely matches that of various reanalysis products relative to CMIP5 (Priestley et al. 2020). Furthermore, the mean SH midlatitude circulation has also shown clear improvements, with reductions in biases from CMIP3 through to CMIP5 (Bracegirdle et al. 2013), and more recently in CMIP6, with the mean jet latitude in summer now being situated within 0.5° of that found in the latest fifth generation ECMWF reanalysis (ERA5, Bracegirdle et al. 2020). It is not just the atmospheric circulation where improvements have been noted from CMIP5 to CMIP6. Improvements have been found in the surface temperature distribution, precipitation, ITCZ structure, and also the cloud radiative properties (Bock et al. 2020; Tian and Dong 2020), all of which may contribute to the reduction of storm track biases in CMIP6.

The large equatorward bias in the SH circulation has been commonly linked to biases in SSTs and an underestimation of atmospheric temperature gradients across a number of generations of climate models (e.g. Trenberth and Fasullo 2010; Ceppi et al. 2012; Sallée et al. 2013; Wang et al. 2014). Recently, Garfinkel et al. (2020) linked the latitude of the eddy-driven jet to the representation of Aghulas Current, with models that have a weak Aghulas return current featuring a more equatorward jet. Two other recent studies (Curtis et al. 2020; Wood et al. 2020) have offered differing hypotheses as to why there has been a reduction in jet latitude bias from CMIP5 to CMIP6. Curtis et al. (2020) discuss that it is a result of improvements in model resolution, whereas Wood et al. (2020) suggest that variations in SST are the leading driver of the change.

Biases in Southern Ocean SST have been shown to be driven by biases in the atmospheric net surface shortwave flux (Hyder et al. 2018) resulting from the misrepresentation of cloud properties, specifically the shortwave cloud radiative effect (SWCRE; Ceppi et al. 2012; Grise and Polvani 2014). The SWCRE is commonly too weak, leading to a net heating of the SH. Biases in the SWCRE modify the strength of SST and midlatitude temperature gradients and hence hemispheric baroclinicity (Ceppi et al. 2012), but have also been shown to have an impact on the temperature structure of the atmosphere through radiative absorption (Li et al. 2015). These longstanding biases have been noted as an area for specific improvement for CMIP6 (Stouffer et al. 2017), as the shortwave cloud feedback has significant implications for the strength of the equilibrium climate sensitivity (Zelinka et al. 2020). So far several studies have demonstrated reduced biases in the newest model generations (Bock et al. 2020; Mauritsen et al. 2019; Kawai et al. 2019), however despite some reductions the CMIP6 multi-model mean has been shown to suffer from the same deficiencies as CMIP5 (Grise and Kelleher 2021).

Another long-standing bias that has not improved from CMIP5 to CMIP6 is the positive track density bias to the south of Australia (Priestley et al. 2020), which is associated with the split jet structure in this region and over New Zealand (Bals-Elsholz et al. 2001). The split jet is a feature that is simulated poorly in climate models, with an overly strong sub-tropical component, and a too weak polar component (Grose et al. 2016; Patterson et al. 2019). The representation of the split jet is partly driven by Antarctic orography (James 1988) and recently Patterson et al. (2020) linked the split jet bias in an idealized GCM to the representation of Antarctic orography affecting the eddy momentum fluxes in this region. Biases in the orographic wave drag have previously been linked to circulation biases in CMIP5 models (Pithan et al. 2016), as well as Rossby waves originating in the Indian Ocean which have been shown to alter the structure of the storm track to the south of Australia (Inatsu and Hoskins 2004, 2006).

Understanding the origin of long-standing biases and reasons for their persistence is vital not just for future model development, but also for having confidence in model simulations and for understanding whether any systematic errors have an influence on future projections. The results presented herein aim to demonstrate linkages in the large-scale atmosphere-ocean system and to act as a framework for future scientific investigation. The science questions addressed in this study are as follows:

- Can the CMIP6 prescribed SST experiments (i.e. AMIP; Gates et al. 1999; Eyring et al. 2016) help to explain some of the coupled storm track biases in the SH?

- Can reduced storm track biases from CMIP5 to CMIP6 be associated with specific model developments?

The paper continues as follows. Section 2 describes the data and methods used for this work. Section 3 presents the results and findings. Finally, in section 4 the key points of this work and its implications in the wider scientific context will be discussed.

2. Data and Methods

a. Datasets

1) CMIP6 Models

In this study the CMIP6 models covering the historical period are used. The *historical* and *amip* model runs are analyzed covering the period from 1979-2014. Focus will be on the December, January, February (DJF) and June, July, August (JJA) periods, representing the SH summer and winter seasons respectively. In total there are 24 models analyzed that have provided data from both a coupled atmosphere-ocean *historical* run and an atmosphere-only *amip* run for the required variables at 6-hourly temporal resolution. A full list of the models analyzed can be found in Table 1. The *amip* experiments are forced by observed SSTs and sea ice concentration and a full explanation of the differences between the experiments can be found in Eyring et al. (2016). Throughout this study the coupled models from the *historical* experiments will be referred to as the CMIP6 models, and the atmosphere-only models from the *amip* experiment will be referred to as the AMIP6 models. Monthly mean data are used to investigate biases in the large-scale fields. For all models only a single ensemble member (*r1i1p1f1* or lowest available) is analyzed.

In some instances models will be separated between those of high and low resolution, for both the atmospheric and oceanic component. For the atmospheric resolution separation the distinction of Priestley et al. (2020) is used and models with a nominal atmospheric resolution (see Taylor et al. 2017) of 100 km are classed as 'high' resolution and those of 250 km are 'low' resolution.

2) CMIP5 Models

The CMIP5 models, which are the same as those used in Priestley et al. (2020) (see also Table S1), provide a benchmark for the CMIP6 models. Of the 26 coupled CMIP5 models employed for this analysis, 19 of them have corresponding *amip* runs. For all models data is used covering the period 1979-2005. Tests have been performed using the 1979-2005 period for the CMIP6 models, with no discernible differences found compared to the data period described above. As with the

CMIP6 models, the coupled models will commonly be referred to as the CMIP5 models, with the atmosphere-only variants being referred to as the AMIP5 models.

Model Name	Institution	Atmospheric Resolution	
		Horizontal	Vertical
ACCESS-CM2	CSIRO-ARCCSS; Commonwealth Scientific and Industrial Research Organisation, Australian Research Council Centre of Excellence for Climate System Science, Australia	N96; 192×144; 250km	85 levels to 85 km
ACCESS-ESM1-5	CSIRO; Commonwealth Scientific and Industrial Research Organisation, Australia	N96; 192×144; 250km	85 levels to 85 km
BCC-CSM2-MR	BCC; Beijing Climate Center, China	T206; 320×160; 100km	46 levels to 1.46 hPa
CMCC-CM2-HR4	CMCC; Fondazione Centro Euro-Mediterraneo sui Cambiamenti Climatici, Italy	288×192; 100km	26 levels to ~2 hPa
CMCC-CM2-SR5	CMCC; Fondazione Centro Euro-Mediterraneo sui Cambiamenti Climatici, Italy	288×192; 100km	30 levels to ~2 hPa
CNRM-CM6-1-HR	CNRM-CERFACS, Center National de Recherches Meteorologiques, center Européen de Recherche et de Formation Avancée en Calcul Scientifique, France	T359; 720×360; 100km	91 levels to 78.4km
EC-Earth3	EC-Earth-Consortium	TL255; 512×256; 100km	91 levels to 0.01 hPa
EC-Earth3-Veg	EC-Earth-Consortium	TL255; 512×256; 100km	91 levels to 0.01 hPa
GFDL-CM4	NOAA-GFDL; National Oceanic and Atmospheric Administration, Geophysical Fluid Dynamics Laboratory, USA	C96; 360×180; 100km	33 levels to 1 hPa
HadGEM3-GC3.1-LL	MOHC; Met Office Hadley Centre, UK	N96; 192×144; 250km	85 levels to 85 km
HadGEM3-GC3.1-MM	MOHC; Met Office Hadley Centre, UK	N216; 432×324; 100km	85 levels to 85 km
IPSL-CM6A-LR	IPSL; Institut Pierre Simon Laplace, France	N96; 144×143; 250km	79 levels to 40 km
KACE-1-0-G	NIMS-KMA; National Institute of Meteorological Sciences/Korea Meteorological Administration, Republic of Korea	N96; 192×144; 250km	85 levels to 85 km
KIOST-ESM	KIOST; Korea Institute of Ocean Science and Technology, Republic of Korea	C48; 192×96; 250km	32 levels to 2 hPa
MIROC-ES2L	MIROC; MIROC Consortium (JAMSTEC, AORI, NIES, R-CCS), Japan	T42; 128×64; 500km	40 levels to 3 hPa
MIROC6	MIROC; MIROC Consortium (JAMSTEC, AORI, NIES, R-CCS), Japan	T85; 256×128; 250km	81 levels to 0.004 hPa
MPI-ESM1-2-HR	MPI-M, DWD, DKRZ; Max Planck Institute for Meteorology, Deutscher Wetterdienst, Deutsches Klimarechenzentrum, Germany	T127; 384×192; 100km	95 levels to 0.01 hPa
MPI-ESM1-2-LR	MPI-M, AWI; Max Planck Institute for Meteorology, Alfred Wegener Institute, Germany	T63; 192×96; 250km	47 levels to 0.01 hPa
MRI-ESM2-0	MRI; Meteorological Research Institute, Japan	TL159; 320×160; 100km	80 levels to 0.01 hPa
NESM3	NUIST; Nanjing University of Information Science and Technology, China	T63; 192×96; 250km	47 levels to 1 hPa
NorESM2-LM	NCC; NorESM Climate Modelling Consortium, Norway	144×90; 250km	32 levels to 3 hPa
SAM0-UNICON	SNU; Seoul National University, Republic of Korea	288×192; 100km	30 levels to ≈2 hPa
TaiESM1	AS-RCEC; Research Center for Environmental Changes, Academia Sinica, Taiwan	288×192; 100km	30 levels to ≈2 hPa
UKESM1-0-LL	UKESM Consortium (MOHC, NERC, NIMS-KMA, NIWA)	N96; 192×144; 250km	85 levels to 85 km

TABLE 1. List of CMIP6/AMIP6 models that have been used in this study. Columns 3 and 4 indicate the horizontal and vertical resolution of the atmospheric component of the model. Any spectral models are first stated by their truncation type and number. ’T’ stands for triangular truncation, ’TL’ stands for triangular truncation with linear Gaussian grid. The models with ’C’ refers to a cubed-sphere finite volumes model, with the following number being the number of grid cells along the edge of each cube face. Models with ’N’ refer to the total number of 2 grid point waves that can be represented in the zonal direction. Following any grid specification is the dimensions of the model output on a gaussian longitude x latitude grid. The resolution stated in kilometres is the stated nominal resolution of the atmospheric component of the model from Taylor et al. (2017).

3) Reanalysis

As a reference to real-world atmospheric variability, the ERA5 reanalysis (Hersbach et al. 2020) is used for comparison with the CMIP5 and CMIP6 models. ERA5 data spans the period from January 1979 up to the near present, with the period 1979-2014 used to provide a consistent comparison period for the CMIP6/AMIP6 models. The ERA5 data are output at 0.28°× 0.28° (~31 km) spatial resolution. Data are used at various output frequencies with feature tracking run on 6-hourly vorticity fields and monthly-to-seasonal averages used for other large scale fields (see below). For ERA5 and the CMIP5 and CMIP6 models described above, all large-scale analyses are performed on the native grids that the data are provided on, the data is then interpolated onto a

$1°\times 1°$ grid for the purposes of visualization.

There are of course differences between numerous reanalysis products with regards to the storm tracks (Hodges et al. 2011) and other large-scale atmospheric variables (e.g. Mooney et al. 2011; Trenberth et al. 2011; Lindsay et al. 2014). Newer generation reanalysis products have been shown to be more consistent in their state of the storm track (Priestley et al. 2020), and therefore in most instances only ERA5 will be used as a reference. However, for a more comprehensive estimation of the real-world cyclogenesis rate and cyclogenesis latitude, both the MERRA2 (Gelaro et al. 2017) and JRA-55 (Kobayashi et al. 2015) reanalyses have been employed alongside ERA5 for the same time period.

4) CERES

In calculations of the shortwave cloud radiative effect (SWCRE) the Clouds and the Earth's Radiant Energy System (CERES) Energy Balanced and Filled (EBAF) Top-of-Atmosphere (TOA) Edition-4.0 Data Product (Loeb et al. 2018) is used to validate the CMIP5 and CMIP6 data. Due to the reduced availability of CERES data and overlap with model data, this data set is analyzed in monthly mean format covering the period 2000 through 2014.

b. Feature Tracking

For the identification and tracking of cyclones the method of Hodges (1995, 1999) is used. This method uses 850 hPa relative vorticity as the input variable, which allows for a reduced influence of the background state on cyclonic features and focuses on smaller spatial scales. The relative vorticity field is first truncated to T42 resolution with all planetary wavenumbers (5 and below) removed. This ensures tracking and cyclone identification is performed on a common resolution despite the varying input resolutions of the model data and reanalysis. Cyclones are initially identified as minima on a polar stereographic projection that exceed $1\times10^{-5}s^{-1}$ (intensity scaled by -1). Following completion of the tracking cyclones are retained that travel at least 1000 km and have a lifetime of at least 48 hours. This ensures the focus is on long-lived and mobile synoptic systems.

Cyclone track density is calculated using spherical non-parametric estimators from the individual cyclone tracks (Hodges 1996). In cases where cyclone genesis and lysis latitude are quantified this is taken as the latitude of the first and last (respective) timestep that the cyclone is identified. For determining the poleward propagation of cyclones the latitude difference between the 9th and 1st timestep (first 48 hours of lifecycle) of the cyclone track is taken.

c. Metrics

To further explore the large-scale climate of the CMIP models a number of diagnostics are used which require manipulation of the raw model output. These metrics are the same as in Priestley et al. (2022) and are documented below.

1) Temperature Gradients

Temperature gradients are calculated using the potential temperature (θ) on pressure levels. Gradients that are used are the meridional gradient of potential temperature as calculated by the Iris package (Met Office 2010 - 2013) and gradients are quoted in units of K degree^{-1}.

2) Static Stability

The static stability is quantified in terms of the Brunt-Väisälä frequency (N^2) calculated on pressure levels (equation 1).

$$N^2 = \frac{-pg^2}{RT\theta}\frac{d\theta}{dp} \tag{1}$$

The static stability is calculated for the lower troposphere with N^2 covering the 700-850 hPa layer. T and θ are the 700-850 hPa average temperature and potential temperature respectively. $\frac{d\theta}{dp}$ is the vertical gradient in θ, calculated across the 700-850 hPa layer.

3) Eady Growth Rate

The Eady Growth Rate (EGR) is a description of the baroclinicity of the atmosphere and combines the two diagnostics described above. For this work the EGR will be a measure of the lower tropospheric baroclinicity and is defined in equation 2.

$$EGR = 0.31 f \frac{\left|\frac{\partial T}{\partial y}\right|}{\sqrt{N^2}} \tag{2}$$

The temperature gradient ($\left|\frac{\partial T}{\partial y}\right|$) is calculated at 850 hPa and the static stability (N^2) is calculated for the 700-850 hPa layer as detailed in equation 1.

3. Results

a. Cyclone Track Densities and Statistics

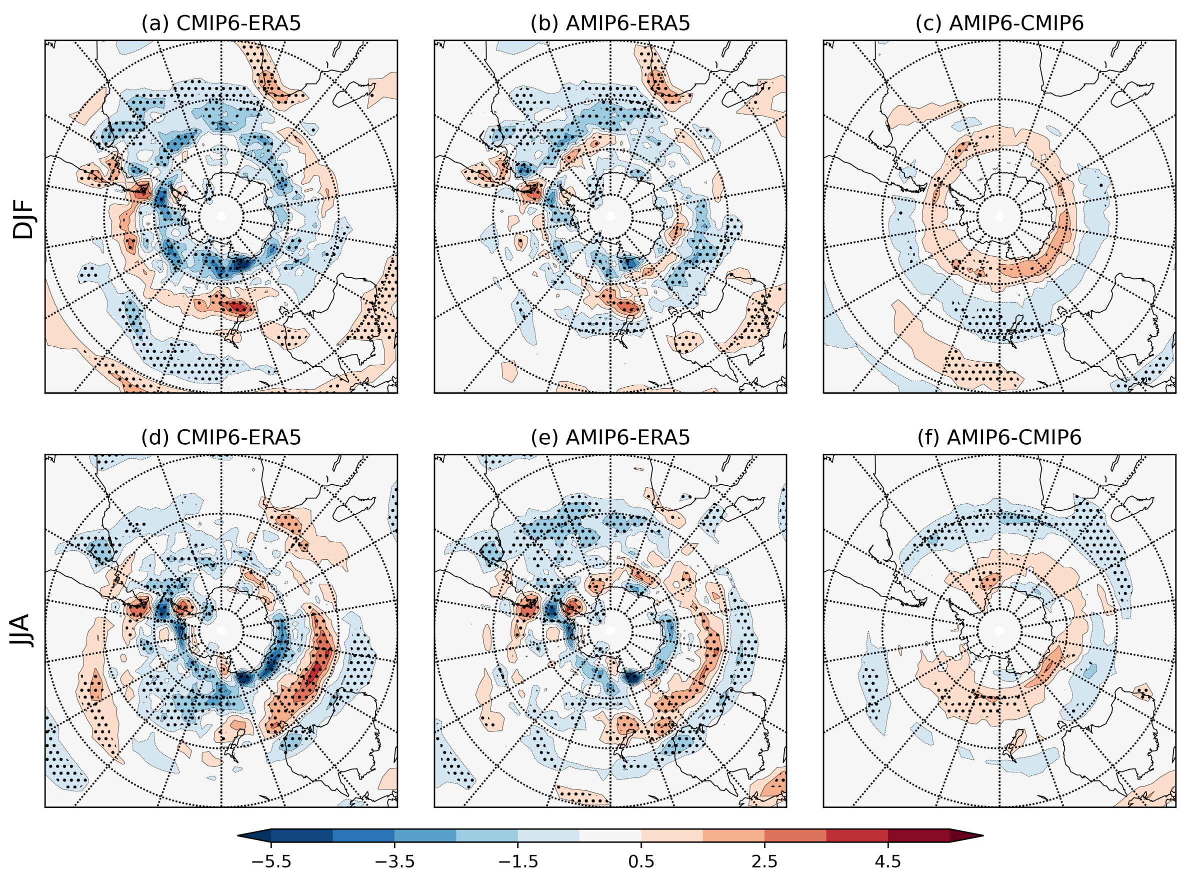

FIG. 1. Track density biases for DJF (a–c) and JJA (d–f) for (a,d) CMIP6 models and (b,e) AMIP6 models relative to ERA5. (c,f) CMIP6-AMIP6. Units are number of cyclones per 5° spherical cap per month. Stippling indicates where more than 80% of models agree on the sign of the error.

In the CMIP6 models, a general improvement in the representation of the SH storm tracks, relative to ERA5, is seen when compared with CMIP5, particularly in DJF (Priestley et al.

2020). Priestley et al. (2020) found that the large equatorward storm track bias of CMIP5 is reduced in CMIP6, with a near total elimination of this feature. Similar patterns are seen in JJA, with a reduction in the equatorward bias noted, however some features still persist, such as an overestimation of track density to the south of Australia where cyclone tracks are too zonal.

Track density biases for the 24 CMIP6 and AMIP6 models are shown in Fig. 1. During DJF, biases in the CMIP6 models (Fig. 1a) are almost identical to those analyzed in Priestley et al. (2020) and indicate an underestimation of tracks in DJF and a slight equatorward bias relative to ERA5. In the AMIP6 models (Fig. 1b) the pattern of biases relative to ERA5 is generally consistent with CMIP6, however there is a poleward shift in the track density (Fig. 1c). Consequently, the previous most evident equatorward biases in DJF across the South Pacific and to the south of New Zealand are mostly eradicated in AMIP6.

The poleward shift of the track density in the AMIP6 models relative to CMIP6 is reflected in the regional cyclogenesis rates (Fig. 2a). During DJF the genesis rate for the whole SH (Fig. 2a) in the AMIP6 models has a very similar median to the CMIP6 models (255 and 256 cyclones per season respectively, not significantly different, Table S2), with slightly larger inter-model spread. The similar genesis rate for the whole hemisphere can be broken down to slightly lower rates of genesis in the equatorward sector (30°S-60°S) and higher rates in the poleward sector (60°S-80°S) in the AMIP6 models relative to CMIP6 (Figs. 2a(ii–iii)). Despite these differences, the genesis density biases (relative to ERA5) are similar between AMIP6 and CMIP6 (Fig. S1d). Some of the differences in genesis density help explain the differences in track density between AMIP6 and CMIP6, for example, there is a reduction in cyclogenesis over New Zealand (Fig. S1d), which is co-located with a reduction in track density (and subsequent poleward shift of tracks, Fig. 1c).

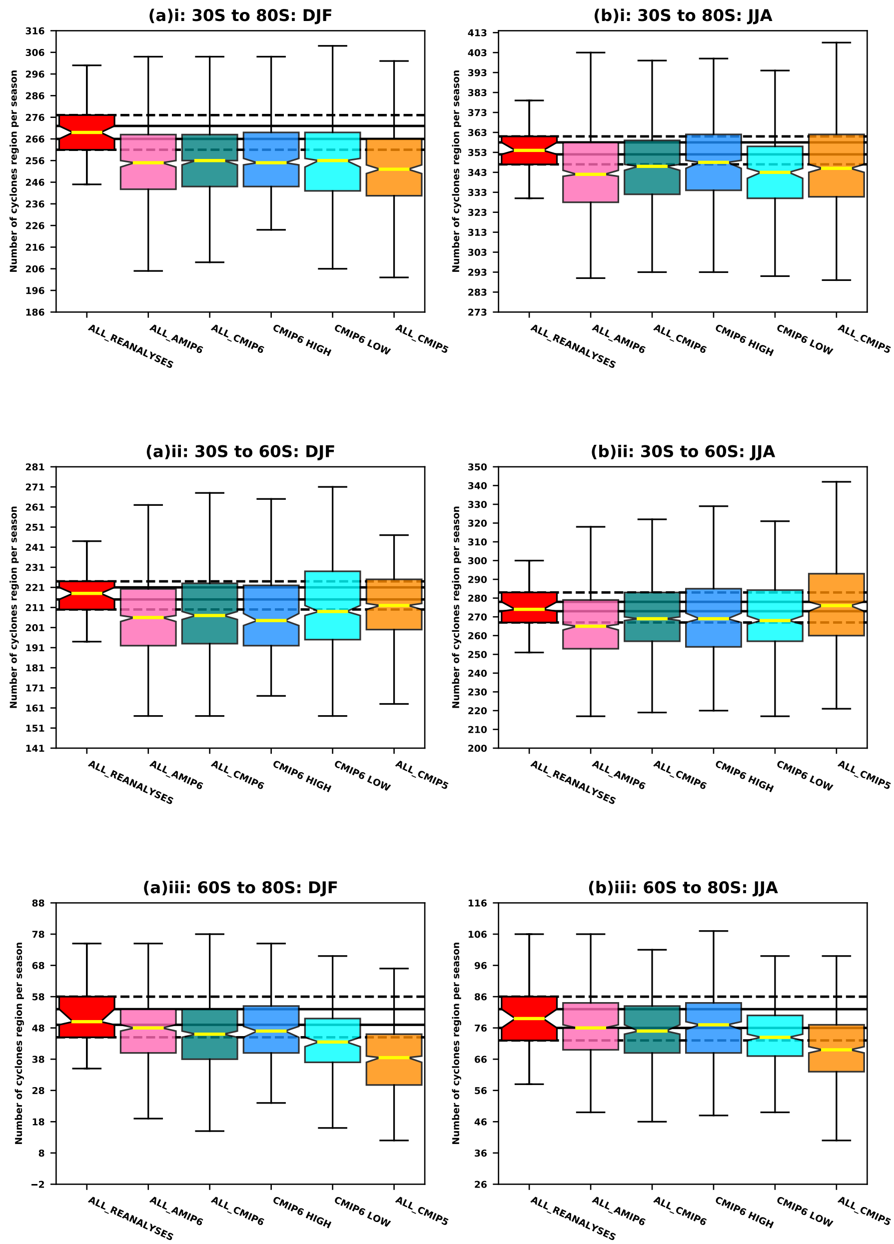

FIG. 2. Boxplots of regional cyclogenesis rates for (a) DJF and (b) JJA. Results are shown for all reanalyses, AMIP6, CMIP6, the two resolution groups of CMIP6, and CMIP5. Solid black lines indicate the uncertainty range of the reanalyses median and dashed black lines signify the 25th-75th percentile range of the reanalyses. Boxes extend to the 25th and 75th percentile respectively with yellow lines indicating the distribution median. Notches around the median show the uncertainty estimate based on 10,000 random samples and whiskers extend to the 10th and 90th percentiles.

The median location of cyclogenesis during DJF in ERA5 and the model groups are plotted in Fig 3a. All model groups are biased by up to 0.5° equatorward relative to the reanalyses, with CMIP5 being the most biased. The CMIP6 models simulate genesis further poleward than CMIP5 by ~0.2° ($p<0.05$), with AMIP6 another 0.1° further poleward, although both are still biased significantly equatorward relative to the reanalyses. The lysis latitude is well simulated by the CMIP6 and AMIP6 models (Fig. 3b), however the CMIP5 models simulate lysis significantly too equatorward according to this metric. Finally, the poleward displacement of cyclones is also well represented in the CMIP6 and AMIP6 models relative to the reanalyses (Fig. 3c). The CMIP5 and AMIP5 simulations tend to underestimate the poleward displacement in the first 48 hours of the cyclone lifecycle by ~0.25°, which is significantly lower than the CMIP6 models. Across all measures the CMIP6/AMIP6 models perform better than the CMIP5/AMIP5 models, with a poleward shift in AMIP relative to CMIP. This suggests that the large improvement seen in track density and the representation of the storm tracks shown in Priestley et al. (2020) has occurred through model developments from CMIP5 to CMIP6. Despite the similarities, there is a larger poleward shift from CMIP5-CMIP6 than from AMIP5-AMIP6, with shifts of 0.48° and 0.43° respectively in lifetime average latitude.

In the winter season (JJA), a similar pattern of track density biases in the CMIP6 and AMIP6 models is evident (Fig. 1d–f). However, the highest track density, as in DJF, is improved in AMIP6 through a poleward shift relative to CMIP6 (Fig. 1f). Other features such as the overly high track density to the southeast of South Africa are reduced. The persistent overestimation of tracks to the south of Australia in the CMIP6 models (as described in Priestley et al. 2020) is also present in the AMIP6 models, although to a lesser extent. Therefore, it is likely that this bias depends upon both the atmosphere/land components of the models and is being amplified through the coupling to an interactive ocean.

In JJA the AMIP6 models also have lower genesis rates than the CMIP6 models from 30°S-60°S (Fig. 2b(ii)) and higher genesis rates from 60°S-80°S (Fig. 2b(iii)). Overall, there are significantly ($p<0.05$) fewer cyclones in JJA in AMIP6 models compared to CMIP6 (medians of 342 and 346 cyclones per season respectively; Fig. 2b(i)). In JJA there is an underestimation of track density from the east coast of South America along 40°S toward South Africa in AMIP6 relative to CMIP6 (Fig. 1f), which represents an even larger underestimation of track density relative to ERA5. This underestimation of track density is coincident with a robust underestimation of genesis density (Fig. S1h). Interestingly, there are minimal differences in genesis rate to the south of Australia in either CMIP6 or AMIP6 relative to ERA5, or from CMIP6 to AMIP6 (Figs. S1f–h). This suggests that the robust track density bias in this region (Fig. 1d,e) is unrelated to the number of cyclones and instead may be driven by errors in cyclone paths being too zonal.

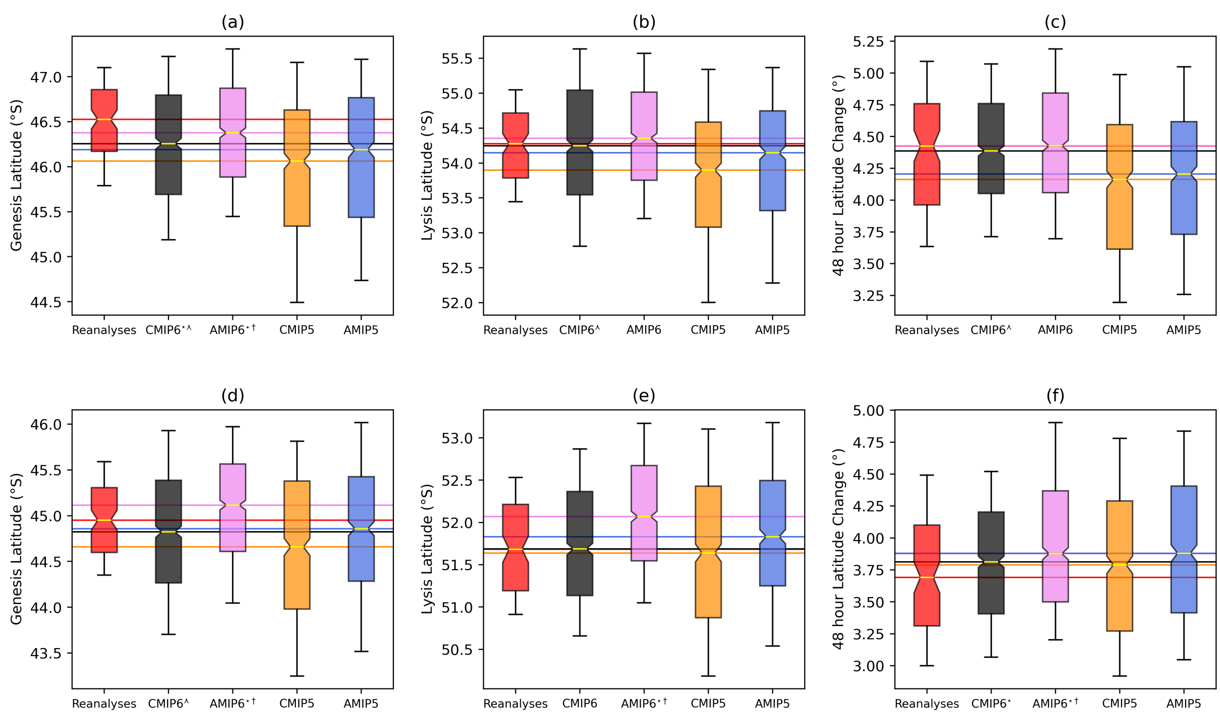

FIG. 3. Boxplots of annual mean cyclogenesis latitude (a,d), cyclolysis latitude (b,e), and cyclone 48-hour latitude change (c,f) for Reanalyses, CMIP6, AMIP6, CMIP5, and AMIP5 in DJF (a–c) and JJA (d–f). Horizontal coloured lines indicate the median value for each model distribution. Boxes extend to the 25th and 75th percentile respectively with yellow lines indicating the distribution median. Notches around the median show the uncertainty estimate based on 10,000 random samples and whiskers extend to the 10th and 90th percentiles. In the labels ⋆ indicates where the model group is significantly different from the reanalyses, † indicates where AMIP6 and CMIP6 are significantly different, and ∧ indicates where CMIP6 and CMIP5 are significantly different. Significance tests performed using a Mood's Median test and quoted at the 5% level.

In JJA the differences in genesis latitude, lysis latitude, and cyclone poleward movement between the CMIP5, CMIP6, and their AMIP counterparts is similar to DJF (Figs. 3d–f). The median genesis latitude continues to be biased equatorward in CMIP5 and CMIP6, although genesis in CMIP6 occurs significantly further poleward than CMIP5, with less than half the bias. The cyclogenesis latitude is displaced significantly poleward in AMIP6 relative to CMIP6, which agrees with Figs. 1 and 2, although the genesis latitude in the AMIP6 models is ~0.1° poleward of the reanalyses (Fig. 3d). The lysis latitude is very well represented in CMIP5 and CMIP6, with a continued poleward bias in AMIP6 relative to ERA5 (Fig. 3e). Finally, for the poleward displacement of the cyclones, all model groups perform similarly but are biased with up to ~0.2° more poleward movement than the reanalyses (Fig. 3f). For most of the metrics in Fig. 3d–f the models produce good results relative to the reanalyses and, at all times, there is considerable overlap in their inter-quartile ranges.

b. Poleward Shift of the Storm Tracks

The largest change from CMIP5 to CMIP6 is the large improvement in the latitudinal bias of the storm track (particularly for DJF) leading to a storm track that is almost unbiased in latitude relative to ERA5 (Priestley et al. 2020; Bracegirdle et al. 2020; Curtis et al. 2020). The drivers of this improvement from CMIP5 to CMIP6, and the further reduction in the bias in AMIP6 models, will be explored below.

In DJF there is a large positive SST bias around Antarctica in the CMIP6 models (Fig. 4b) relative to ERA5 (Fig. 4a), which has persisted from CMIP5 (Fig. 4c). The SST biases in Fig. 4 are substantially different than those shown in OMIP experiments (Tsujino et al. 2020), indicating it is likely that the SST biases are driven by processes occurring in the atmospheric component of the models. For CMIP5 models, the warm bias in the high latitude Southern Ocean has been demonstrated to arise from positive biases in the cloud-related shortwave fluxes, which result in associated errors in atmospheric net heat flux (Ceppi et al. 2012; Hyder et al. 2018). These biases have been shown to be linked to insufficient cloudiness and optical depth within the cold sectors of cyclones (Grise and Polvani 2014; Williams et al. 2013; Bodas-Salcedo et al. 2014; Govekar et al. 2014; Williams and Bodas-Salcedo 2017). As the CMIP6 models

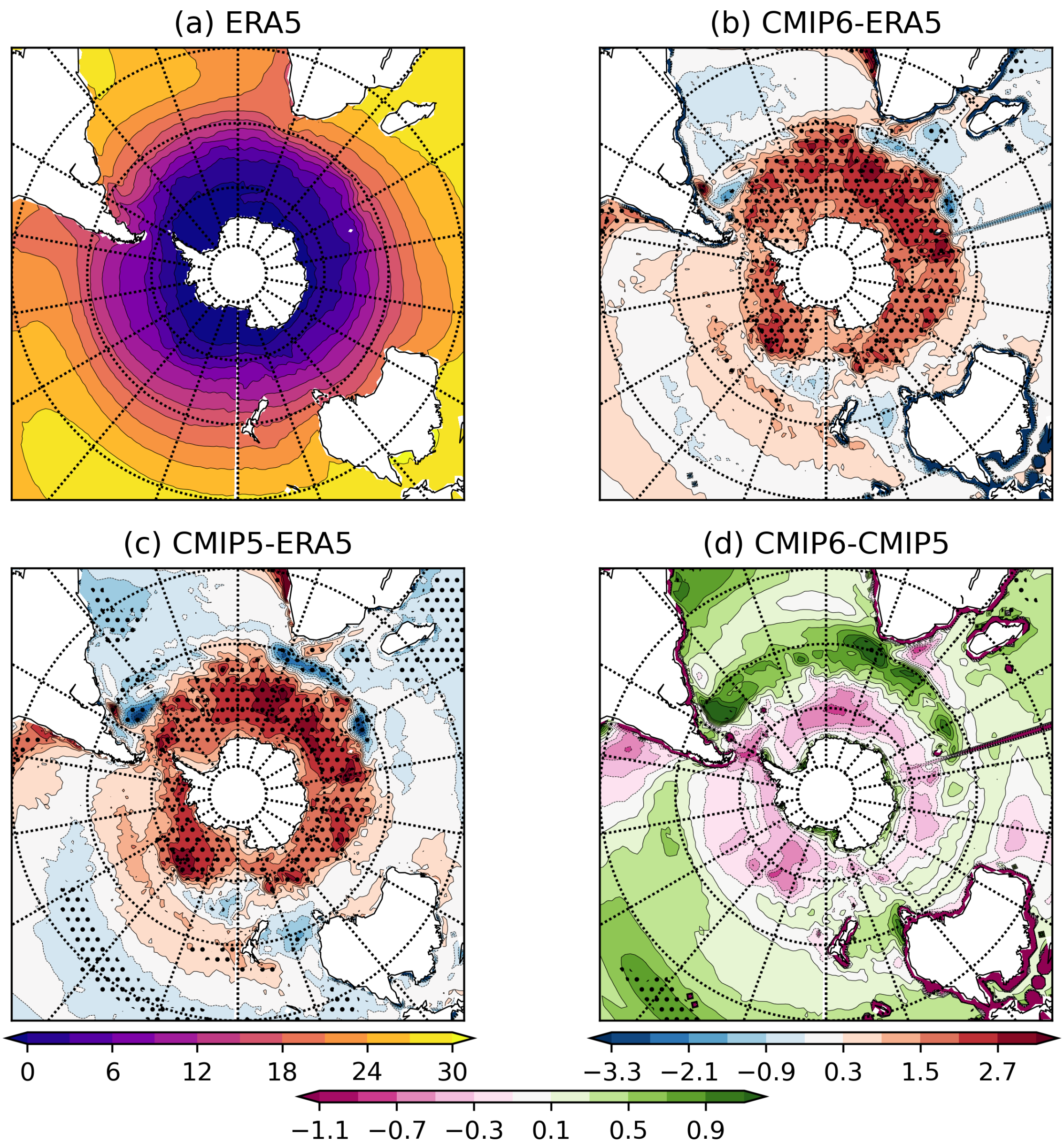

FIG. 4. DJF averaged sea surface temperature (SST) for (a) ERA5 (b) CMIP6-ERA5, (c) CMIP5-ERA5, and (d) CMIP6-CMIP5. Stippling indicates where there is 80% model agreement on the sign of the bias. Units are °C. Data are taken from the Sea Surface Temperature (*tos*) CMIP variable.

continue to have a high-latitude Southern Ocean that is too warm relative to observations, it is likely that the same biases in the cloud-related shortwave fluxes are still present. To demonstrate this the zonal mean differences in the SWCRE for CMIP6 (red line) and CMIP5 (blue line) relative to CERES are plotted in Fig. 5a. In the CMIP6 models the SWCRE is still too weak[1] relative to CERES at high latitudes (i.e. poleward of 55°S, red line in Fig. 5a), and therefore the process driving the warm SSTs in the CMIP5 models appears unimproved in the CMIP6 models.

At mid-to-lower latitudes (from approximately 40°S-50°S) CMIP6 SSTs are generally up to 1°C higher than in CMIP5 (Fig. 4d), particularly in the South Atlantic and Indian Ocean sectors. The SSTs in this sector are particularly important for modulating the latitude of the storm track in CMIP6 models (as indicated by the significant linear regression in Fig. 6a), with warmer SSTs associated with a more poleward storm track. This is not something that is seen in CMIP5 models (Fig. 6b). This 40°S-50°S latitude band is where the largest differences in the magnitude of the SWCRE bias from CMIP5 to CMIP6 are seen, with CMIP6 models having a smaller bias and less negative SWCRE compared to CMIP5 (Fig. 5a). This reduced bias is likely contributing to the higher midlatitude SSTs in CMIP6. It is worth noting here that the increase in SSTs (CMIP6 relative to CMIP5) is largely the result of the amelioration of cold biases present in the CMIP5 models (particularly in the region of the Agulhas current retroflection, see Fig. 4).

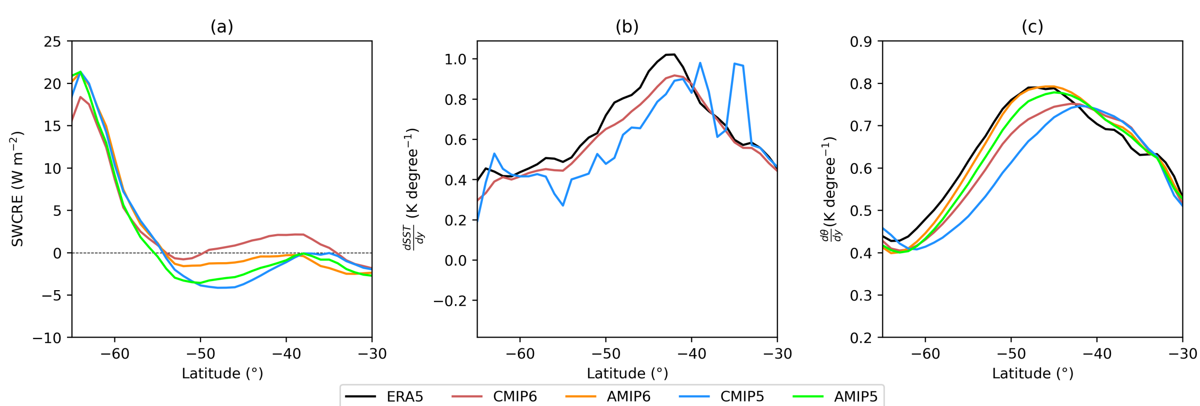

FIG. 5. The ensemble zonal mean difference in (a) SWCRE (W m^{-2}), (b) zonal mean SST gradient (K degree latitude^{-1}) and (c) zonal mean 850 hPa potential temperature gradient (K degree latitude^{-1}) for CMIP6 (red line), AMIP6 (orange line), CMIP5 (blue line) and AMIP5 (green line). The differences are for (a) model ensemble mean minus CERES.

[1] as the "background state" SWCRE is negative in both the models and CERES, a positive bias implies that CMIP6 SWCRE is "less negative" (i.e. weaker) than that of CERES and vice versa

The pattern of positive high-latitude and negative midlatitude SST biases in CMIP6 and CMIP5 (discussed above) causes the SST gradient to be weaker poleward of 40°S in both ensembles relative to ERA5 (Fig. 5b). Nevertheless, the midlatitude SST gradient in CMIP6 is stronger than CMIP5 between approximately 40°S-60°S (see Fig. 5b). A good representation of the strong SH midlatitude SST gradient in the models is important as it acts to maintain baroclinicity in the atmosphere (Nakamura et al. 2008; Nakayama et al. 2021). A weak temperature gradient may reduce the midlatitude baroclinicity and thereby reduce the strength of the storm track (Graff and LaCasce 2014; Garfinkel et al. 2020; Kajtar et al. 2021; Nakayama et al. 2021). It is therefore important to evaluate whether the biases in the SST gradient (Fig. 5b) are also apparent in the atmosphere. The zonal mean 850 hPa potential temperature (θ_{850}) gradient is plotted for ERA5 (black line), CMIP5 (blue line) and CMIP6 (red line) in Fig. 5c. The CMIP6 and CMIP5 models generally feature a weaker atmospheric temperature gradient in the midlatitudes relative to ERA5 (Fig. 5c) as a result of temperatures being too high surrounding Antarctica. As with the SST gradient, the biases in the θ_{850} gradient are smaller in CMIP6 than CMIP5, relative to ERA5. The stronger θ_{850} gradient in CMIP6 relative to CMIP5 between 40°S-60°S (Fig. 5c, red versus blue lines) is likely to be driven by the higher θ_{850} values equatorward of approximately 50°S rather than the (smaller magnitude) reduction in 850 hPa θ adjacent to Antarctica (Fig. S3e).

In order to further evaluate the role of the SST biases on the atmospheric temperature gradient and storm tracks, data from the AMIP6 simulations are used. As the SSTs in AMIP6 simulations are prescribed from observations, the biases in the midlatitude SST gradient should be negligible and any errors should be primarily the result of atmospheric processes. In the AMIP6 models, a stronger θ_{850} gradient is seen compared to CMIP6 models (Fig. 5c, orange versus red lines), although the θ_{850} gradients are weaker relative to ERA5 poleward of 50°S (Fig. 5c, black line). The larger midlatitude temperature gradient in AMIP6 is the likely driver of the more poleward location of the storm track relative to CMIP6 (see Fig. 1c and Priestley et al. 2020) and the largest increases in the 850 hPa zonal wind (Fig. S2c). The increase in θ_{850} gradient in AMIP6 relative to CMIP6 is driven by reducing the high latitude temperature bias (Fig. S3c) and not through increasing lower latitude temperatures, as is the case from CMIP5 to CMIP6 (Fig. S3e). Nevertheless, there are still clearly biases in the representation of the SH storm track in the AMIP6 simulation (Fig. 1c), which are not resolved by using observed SSTs. Moreover, as both the AMIP5 and AMIP6 models are forced by the same prescribed SSTs, there should be minimal influence from the ocean state and therefore one would not expect large differences in the midlatitude temperature gradient. However, there is a clear increase in the temperature gradient in AMIP6 models, relative to AMIP5 (Fig. 5c). This increase in temperature gradient is associated with higher temperatures in the lower troposphere from 40°-50°S in similar locations to the biases in the coupled models (black contours Fig. S3e and f). Radiative processes have been shown to influence the temperature structure of atmosphere-only models (Li et al. 2015) and, as with the coupled models, the AMIP6 models feature a smaller bias in SWCRE than the AMIP5 models in the midlatitudes (40°-50°S, Fig. 5a). The temperature (and gradient) change from AMIP5 to AMIP6 is geographically very similar to the CMIP5 to CMIP6 change, yet is smaller in magnitude. Therefore, the temperature change from 40°S-50°S has its origins in the atmospheric component of the models, which is then amplified further by the SST biases in the coupled models (as in Hyder et al. 2018).

Overall there has been an improvement in the SH midlatitude temperature gradients (both θ_{850} and SST) from CMIP5 to CMIP6 (Figs. 5b and 5c). This improvement appears to be the result of reducing biases in the SWCRE in the midlatitudes (Fig. 5a). Furthermore, when SSTs are prescribed from observations (AMIP6), the representation of the temperature gradients improve further. These results (SST and θ_{850} gradient improvement) are consistent with the better representation of the storm tracks in CMIP6 relative to CMIP5 (also noted by Bracegirdle et al. 2020), and also AMIP6 relative to CMIP6. There is also a clear improvement of the temperature gradient (Fig. 5c) and jet (Fig. S2f) in AMIP6 relative to AMIP5, despite both experiments using the same SST dataset (as also noted by Curtis et al. 2020). Therefore, improvements in the SST alone cannot explain the improved midlatitude circulation in CMIP6 relative to CMIP5. However, while the location of the jet and mean latitude of cyclogenesis (Fig. 2a) are simulated better in CMIP6/AMIP6 relative to CMIP5/AMIP5, there is still a lack of cyclogenesis events (Fig. 1a and Table S2) in the SH during DJF. Therefore there are still clear problems with the representation of extratropical cyclones in the SH midlatitudes. Further interpretation is given in Section 4.

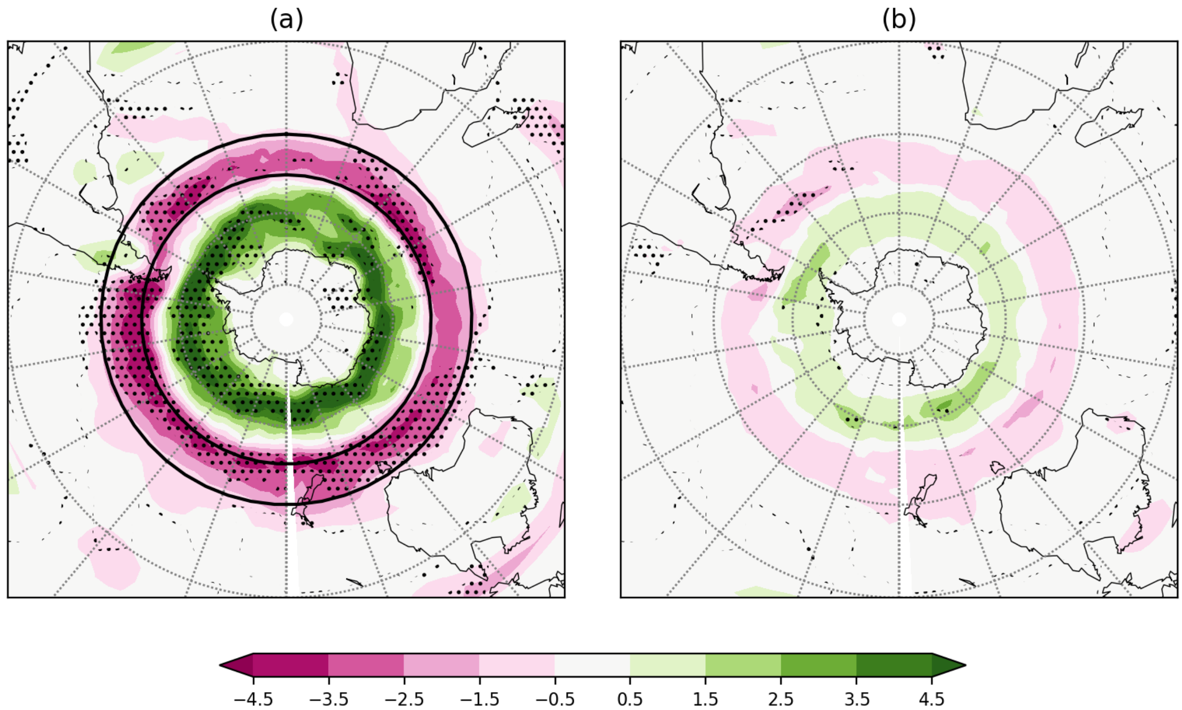

FIG. 6. Linear least-squares grid-point regression slope maps of DJF seasonal mean storm track density, against area averaged SST from 40°S-50°S for (a) CMIP6 and (b) CMIP5. Regression is performed across the model means of the CMIP6 and CMIP5 ensembles respectively. Stippling indicates where regressions are significant at the 5% level. The black box in (a) indicates the region of SSTs used in the regression calculations. Units are cyclones per month K^{-1}.

c. Winter Cyclogenesis Rate

Despite improvements in modeling capabilities from CMIP5 to CMIP6, CMIP6 models continue to underestimate cyclogenesis rate in the SH (Fig. 2b). Unlike in DJF, radiative processes do not have a dominant influence on baroclinicity and therefore the cyclogenesis rate and storm track latitude in JJA. Consequently, we use the Eady Growth Rate (EGR) to examine rates of cyclogenesis in the SH winter. The EGR broadly indicates where the largest track and genesis densities are likely to occur. Positive (negative) EGR biases are a proxy for higher (lower) cyclone track and genesis densities.

1) Eady Growth Rate

In JJA the CMIP6 models feature negative biases of EGR in the South Atlantic sector and to the south of New Zealand and generally higher values around the rest of the hemisphere (Fig. 7b), with a similar pattern of biases in CMIP5 (Fig. 7d). However, the CMIP6 models tend to have lower EGR values around a majority of the SH, relative to CMIP5 (Fig. 7e). The smaller EGR of CMIP6 is consistent with the lower cyclogenesis rate in CMIP6 relative to CMIP5, equatorward of 60°S (Fig. 2b). In the AMIP6 models the EGR is higher than in CMIP6 (Fig. 7c), which is not consistent with the cyclogenesis rate (Fig. 2b).

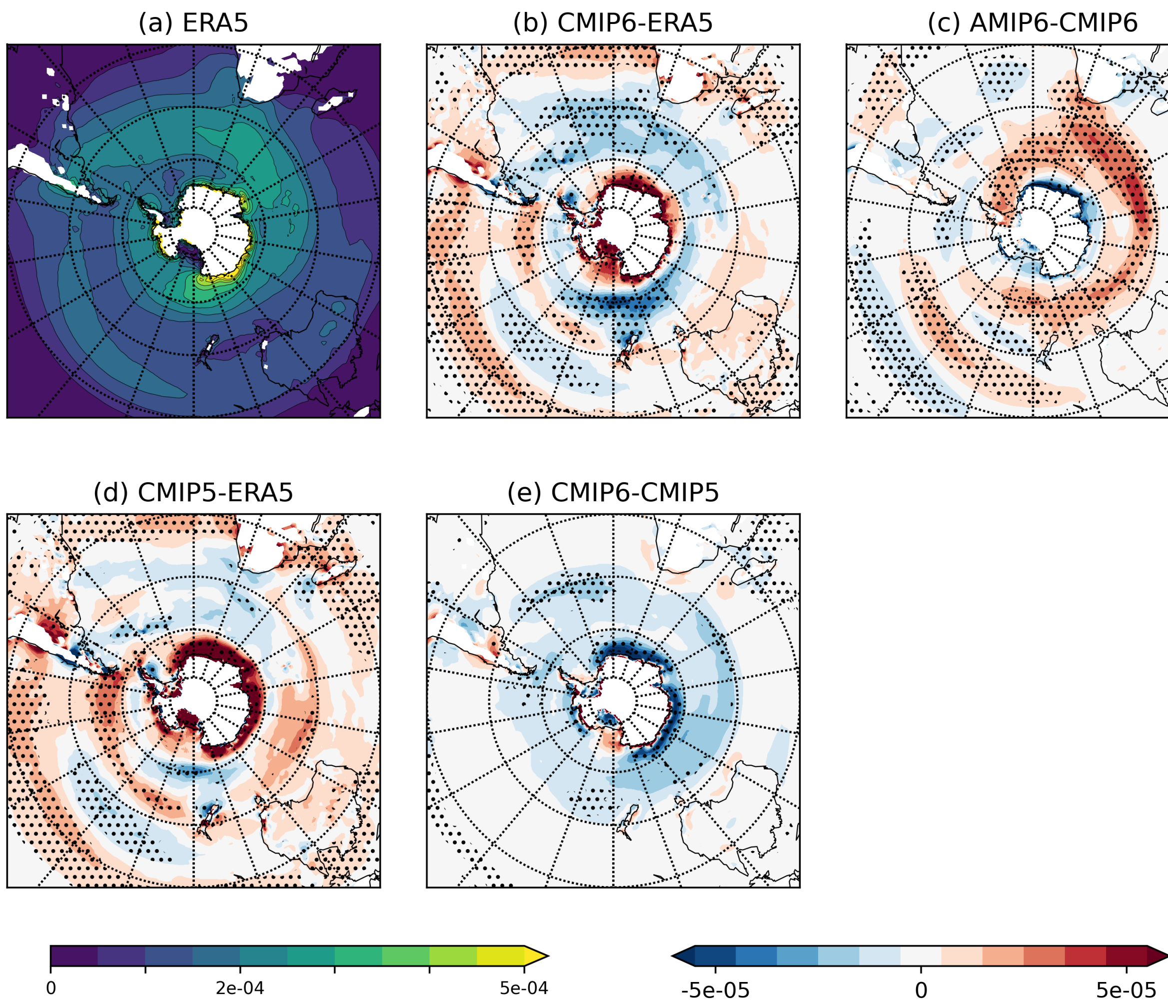

Fig. 7. Eady Growth Rate for JJA for (a) ERA5, (b) CMIP6-ERA5, (c) AMIP6-CMIP6, (d) CMIP5-ERA5, and (e) CMIP6-CMIP5. Units are s^{-1}. Stippling indicates where there is 80% model agreement on the sign of the change.

The differences in EGR, and the related cyclogenesis rates can be understood through inspecting the two components that make up the EGR, the gradient of potential temperature at 850 hPa and the lower tropospheric static stability (see equation 2). For both CMIP5 and CMIP6, a positive relationship is seen between the average static stability from 40°S-70°S and the rate of cyclogenesis in the same region (Fig. 8a). Furthermore, these two fields are positively correlated, which implies that models that are more stable have higher levels of cyclogenesis. This is counter-intuitive as cyclogenesis will typically occur in less stable environments. Reducing the lower-tropospheric stability through an imposed 4K surface heating would not change the temperature gradient, and a lower stability does not appear to influence the cyclogenesis rate in the models (Fig. 8a). It therefore seems unlikely that the static stability is the driving factor behind the lack of cyclogenesis in the CMIP6 models.

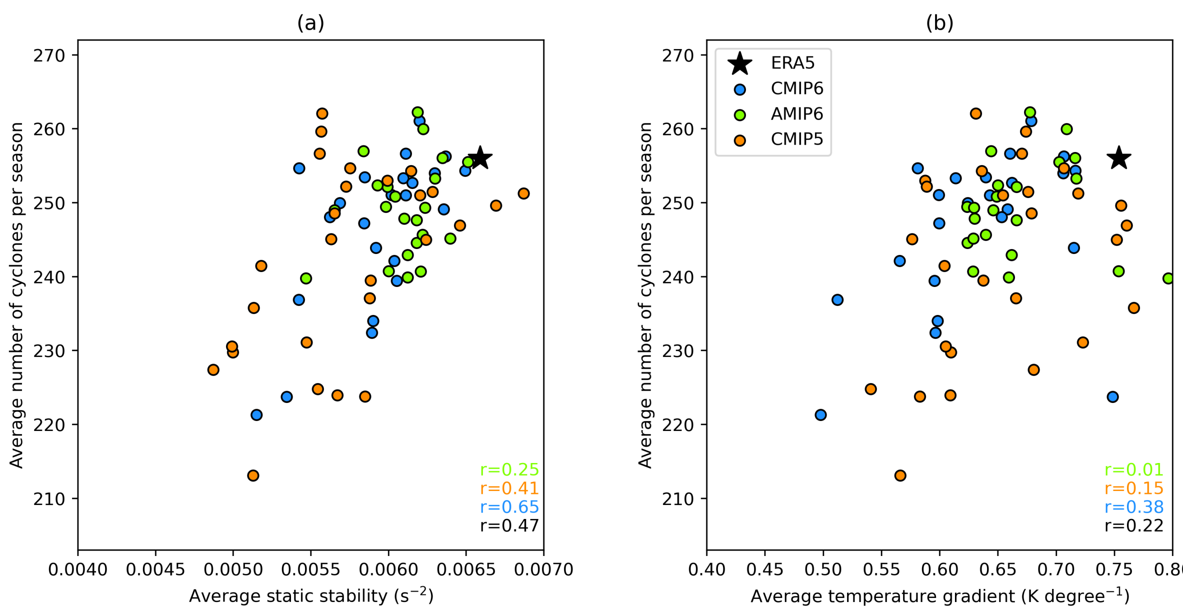

FIG. 8. Scatter plots of (a) lower tropospheric static stability (s^{-2}) and (b) 850 hPa potential temperature gradient (K degree^{-1}) against seasonal cyclogenesis rate. Large-scale fields are averages from 40°S-70°S for CMIP6 (blue), CMIP5 (orange), AMIP6 (green) and ERA5 (black star) in JJA.

The other component of the EGR is the potential temperature gradient associated with vertical wind shear. All model groups, both CMIP and AMIP feature a positive relationship between the θ_{850} gradient and number of cyclones (Fig. 8b), with models that have more cyclones having a stronger temperature gradient. Unlike the stability relationships, this is what would be expected, as stronger temperature gradients that more closely match the reanalysis values would result in a greater number of cyclones. Therefore, it appears that the strength of the temperature gradient, and not the atmospheric stability, is the primary factor controlling the cyclogenesis rate.

This result also suggests that correcting the cause of SST biases in coupled models might improve the stability of the models, but as the stability does not appear to be the controlling factor on cyclogenesis rate, this may not yield any additional cyclogenesis. However, a decrease in SSTs in the most poleward regions would also increase the large-scale temperature gradient (as in Fig. S3c), and therefore increase the rate of cyclogenesis.

d. Persistent South Australian Track Density Overestimation

One bias that has persisted from CMIP5 to CMIP6, and is also present in the AMIP6 models (Fig. 1d–f), is the overestimation of the track density to the south of Australia during JJA. This bias is associated with the bifurcation of the split sub-tropical and polar front jet located in this region (Fig. 9), which models represent poorly (Grose et al. 2016; Patterson et al. 2019). Models tend to have biases from ~90°E-180°E with a too strong subtropical jet along 40°S (most visible at 250 hPa, Fig. S5a), and a polar jet that is too weak along 60°S (most visible at 850 hPa, Fig. 9a). Despite the two jets generally being identified at different pressure levels, the two biases are notable in the CMIP6 and CMIP5 models (Fig. 9b,d, S5b–d) at all pressure levels.

The bias in the zonal wind reflects that of the track density bias of CMIP6 models in Fig. 1d–f and also of CMIP5 models in Fig. 9 of Priestley et al. (2020). The CMIP6 models simulate only a slight poleward shift in the zonal wind south of Australia (Fig. 9e), as in the track density, relative to CMIP5. The AMIP6 models feature a more poleward circulation than in CMIP6 (Fig. 9c), although the zonal bias in this sector still remains (not shown), suggesting that this error may be amplified by SST biases in the coupled models, but ultimately has its roots in the atmosphere or land component of the models.

The better representation of the jet and storm track structure in AMIP6 is a result of a more poleward location of the circulation in JJA relative to CMIP6 (similar but smaller magnitude

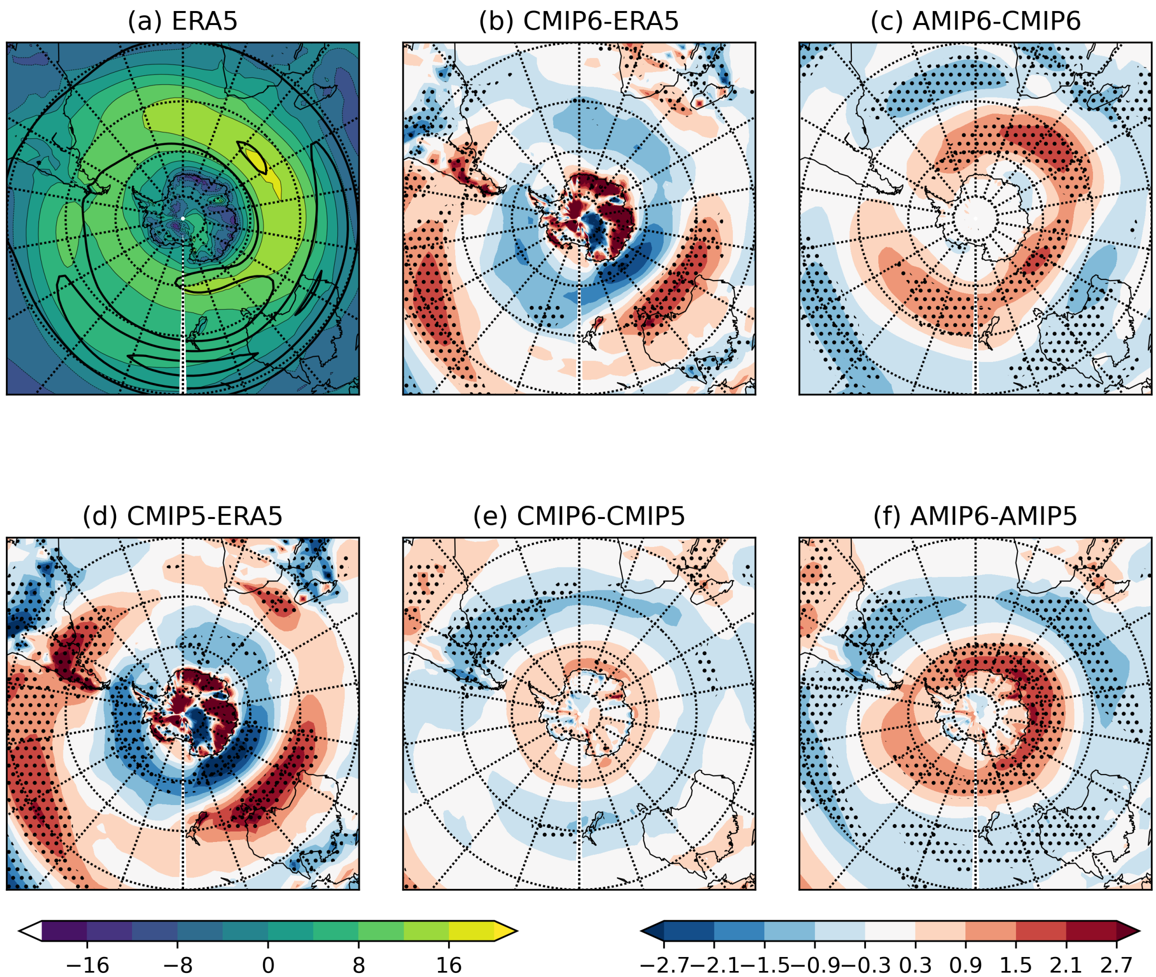

FIG. 9. JJA averaged zonal wind (u) at 850 hPa for (a) ERA5, (b) CMIP6-ERA5, (c) AMIP6-CMIP6, (d) CMIP5-ERA5, (e) CMIP6-CMIP5, and (f) AMIP6-AMIP5. Overlaid black contours in (a) is the 250 hPa ERA5 zonal wind with contours of 24, 36, and 48 m s^{-1}.

as discussed in Bracegirdle et al. 2020). In JJA the SST anomalies of the CMIP6 models are consistent with those in DJF (Fig. 4) and therefore the AMIP6 models have considerably lower atmospheric potential temperature relative to CMIP6 (south of South Africa, poleward of 50°S) when the SSTs are corrected (Fig. S6c). This decrease in potential temperature poleward of 50°S leads to an increase in the temperature gradient from 40°S-50°S in AMIP6 relative to CMIP6 in a very similar pattern to the increase in EGR shown in Fig. 7c from 20°W-100°W. The stronger temperature gradient contributes to shifting the circulation poleward, which may then have downstream impacts on the South Australian sector. Despite this shift, the dominant split jet bias clearly still has an impact on the circulation and track density bias of this region in the AMIP6 models.

The driver of the positive bias in the zonal wind from 100°E-160°E cannot be directly investigated due to the limited output of CMIP6 models and inability to perform interactive experiments, however insight can be gained through examination of the seasonal mean meridional wind (*v*) which appears to display an anomalous standing wave pattern in the CMIP6 models (Fig. 10). Directly to the west of the zonal jet anomaly (Fig. 9b) there is a region of anomalously northwards (positive *v*) motion (along 100°E; Fig. 10a) which contributes to reducing the poleward motion of cyclones downstream of the anomaly. There also appears to be a wave train (denoted by the opposing meridional wind anomalies) extending in an arc from Madagascar to the west coast of South America (Fig. 10a). The origins of this apparent wave train can be estimated from biases in the divergence and velocity potential (Fig. 10b,c). To the southeast of the horn of Africa, positive divergence, and negative velocity potential (relative to ERA5), indicates a possible source of this standing wave pattern.

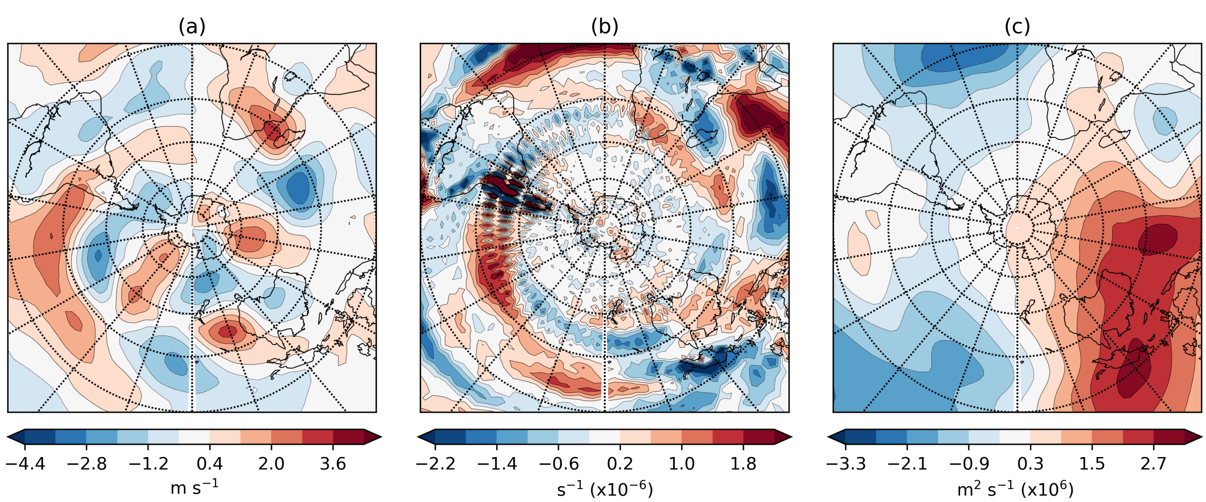

FIG. 10. Circulation biases of CMIP6 relative to ERA5 for (a) meridional wind, (b) divergence, and (c) velocity potential. All variables are shown at 250 hPa and for JJA.

The presence of the split jet has been shown to be associated with Rossby waves originating from upper-level divergence over the Indian Ocean (Inatsu and Hoskins 2004, 2006) and it has been shown that Rossby wave sources are incorrectly modeled in the CMIP5 models (Nie et al.

2019). Based on the divergence pattern and origin of the wave train it is also possible that this wave train could have its origins in the equatorial Atlantic ocean, where biases in the location of the ITCZ (present in CMIP6 models, see Tian and Dong 2020), affect the source of planetary waves. Divergence anomalies across southern Africa could also be a result of incorrect orographic interaction with the mean-flow, which is a long standing problem with GCMs (Inatsu and Hoskins 2004). Recently, Patterson et al. (2020) associated the split-jet bias to the representation of Antarctic orography, and therefore the incorrect representation of the orographic impact on the circulation in the CMIP6 models may be contributing to this bias. The stationary wave pattern in the meridional wind, the divergence, and velocity potential is evident in all models and also in the atmosphere-only simulations for both 5th and 6th generation models.

4. Discussion and Conclusions

In this study the state of the Southern Hemisphere storm tracks has been examined in both coupled and atmosphere-only model simulations from both the 5th and 6th Coupled Model Intercomparison Projects. The influence of ocean biases on model errors and also other large-scale features has been investigated. Furthermore, reasons for improvements from CMIP5 to CMIP6 have been explored. The main conclusions of this work are detailed below.

- AMIP6 models generally show reduced storm track biases relative to CMIP6 models (Fig. 1). AMIP6 models also tend to simulate storm tracks that are located further poleward than in CMIP6, eliminating some of the equatorward bias relative to ERA5 (Fig. 2, 3). Despite these improvements, the overall cyclogenesis rate is biased even lower than CMIP6 (Fig. 2).

- The improved location of the storm track due to a poleward shift from CMIP5 to CMIP6 is associated with increased SSTs and temperatures in the lower troposphere from 40°S-50°S (Fig. 4, S3), which increases the midlatitude temperature gradients (Fig. 5, S3). The AMIP6 models simulate an improvement of the storm track location relative to the AMIP5 models due to increases in the tropospheric temperature with no influence from the underlying ocean state (Fig. 5c).

- The biases in cyclogenesis rates in the SH are primarily associated with increases in atmospheric temperature gradients rather than static stability (Fig. 8). Models that have lower cyclogenesis rates relative to reanalyses have midlatitude temperature gradients that are too weak.

- The overestimation of tracks to the south of Australia in JJA is related to biases in the split jet in the same region, where the sub-tropical jet is too strong. The jet appears to be modulated by a planetary wave train that likely has origins in the equatorial Indian and/or Atlantic Oceans, which weakens the polar component of the split jet (Fig. 10). The presence of the wave train decreases the poleward movement of cyclones forming to the southwest of Australia, driving the track density bias.

One finding from this work is that the CMIP6 models offer an improved representation of the storm track latitude compared to CMIP5 as a result of a poleward shift in temperature gradients and jet latitude. However, despite this apparent improvement, the shift in temperature gradients and circulation appears to be driven by an amelioration of pre-existing CMIP5 biases, particularly in the region of the Agulhas current retroflection, and not through improving the long-standing high latitude Southern Ocean warm biases. Therefore, further attention is required to eliminate these compensating biases that may yield further improvements in storm track representation and have implications for future projections (Kajtar et al. 2021).

With respect to the improvement in the representation of the latitude of maximum zonal wind and cyclogenesis in CMIP6 relative to CMIP5, we have explored three plausible reasons for this:

1. The representation of SSTs within the models, particularly with respect to their variability and geographical distribution of warm and cold areas, are driving the changes in the SH circulation in CMIP6 relative to CMIP5 (Wood et al. 2020).

2. Increased resolution in the CMIP6/AMIP6 generation of models, relative to their CMIP5/AMIP5 counterparts, leads to the SH jet being located more poleward (i.e. better) in the higher resolution CMIP6/AMIP6 simulations (Curtis et al. 2020).

3. Improvements in the representation of clouds and their radiative properties within the models may lead to an improvement in the temperature structure of the whole atmosphere, which

leads to a better representation of the preferred location of baroclinic eddy growth. This has been shown in atmosphere-only models by Li et al. (2015).

It is clear from the analysis provided in Section 3a that it is difficult to truly separate the impact of SST (Wood et al. 2020), resolution (Curtis et al. 2020) and clouds (Li et al. 2015) on the preferred location for extratropical cyclone development and it is likely that each process is playing a role in causing errors in the SH storm tracks. Given the changes in the 850 hPa temperature gradient and the mean cyclogenesis latitude seen in the AMIP6 runs relative to AMIP5 (Figs. 5c and 3a), it is more likely that the processes suggested by Curtis et al. (2020) and Li et al. (2015) (i.e. points 2 and 3 above) are likely to be the main causes. Nevertheless, there is some impact from the SST distribution (Fig. 5b and 6a), which agrees with Wood et al. (2020). Furthermore, the representation of other physical processes (either parametrised or explicitly represented) not discussed in the study may be contributing to the changes in mean state from CMIP5 to CMIP6. The representation of surface drag (Pithan et al. 2016), cloud radiative heating (Voigt and Shaw 2015), and the resolution of the stratosphere (Wilcox et al. 2012) have all been shown to influence the mean state and response of the SH circulation. All these features likely influence the model biases, yet understanding which is playing the dominant role may be key to understanding the biases in extratropical cyclone formation in the SH; however, this is beyond the scope of this paper and is an area for future work.

The atmospheric temperature gradient has been shown to be important for correctly representing the cyclogenesis rate in the Southern Hemisphere (Fig. 8b). As the CMIP6 and AMIP6 models still tend to underestimate the cyclogenesis rate (Fig. 2) it is likely that improvements will be made with increased horizontal resolution. Increasing resolution would likely have beneficial impacts on SST and atmospheric temperature gradients and therefore storm track latitude and cyclogenesis rate, as was suggested by Curtis et al. (2020). However, resolution is not the only important factor when representing extratropical cyclones, which can be seen by comparing cyclogenesis rates in the midlatitude and high latitude bands (Fig. 2 and Priestley et al. 2020) and indicates that the low-resolution CMIP6 (~250 km) models perform similarly to the high-resolution (~100 km) CMIP6 models. Therefore, further work is needed to identify how resolution plays a role in improving the representation of the storm tracks and whether that improvement might be negated by the configuration of a given model.

Going forward, further investigation into the drivers of the SH circulation and storm track biases can be performed utilizing the HighResMIP experiments (Haarsma et al. 2016). These models feature horizontal resolutions of ~25-50km and ocean resolutions of 0.25° and have yielded improvements in numerous global model biases (e.g. Baker et al. 2019; Gutjahr et al. 2019; Roberts et al. 2019). Despite the aforementioned limited improvements with horizontal atmospheric resolution of 100km (Priestley et al. 2020), it may be that increases in resolution to 25-50km in the HighResMIP models yields some benefits. Willison et al. (2013) noted improvements in cyclone moist processes at 20km resolution, which can have feedbacks on large-scale circulation (e.g. Tamarin and Kaspi 2016). Furthermore, orographic features are more accurately represented in high resolution models (Sandu et al. 2019), and improved orographic representation has been shown to reduce circulation biases in the SH (Patterson et al. 2020) and NH (Davini et al. 2021), and may be significantly improved in HighResMIP models.

An additional research avenue would be to investigate the processes leading to the changes in radiative forcing in the latest generation of coupled and atmosphere-only models. Creating specific experiments from which a wide array of variables can be output, the influence from longwave and shortwave radiation and the rates of atmospheric absorption can be quantified. Finally, it has recently been documented by Kajtar et al. (2021) that models with reduced latitudinal biases have less 'capacity for change' under future climate conditions and that models with greater latitudinal storm track/jet biases have stronger climate responses (e.g. Chang et al. 2012; Kidston and Gerber 2010). Therefore, as the CMIP6 models in this study have a reduced equatorward bias, it may be that the magnitude of the poleward shift of storm tracks in the Southern Hemisphere is smaller in CMIP6 than in CMIP5.

Acknowledgments. M. D. K. Priestley and J. L. Catto are supported by the Natural Environment Research Council (NERC) grant NE/S004645/1. D. Ackerley was supported by the Met Office Hadley Centre Climate Programme funded by BEIS and Defra. K. I. Hodges was funded by the United Kingdom's Natural Environment Research Council (NERC) as part of the National Centre for Atmospheric Science. We thank the ECMWF for their ERA5 reanalysis, which is available from the Copernicus Climate Change Service Climate Data Store (https://cds.climate.copernicus.eu/#!/search?text=ERA5&type=dataset). CMIP6 data is publicly available through the Earth System Grid Federation (https://esgf-node.llnl.gov/projects/cmip6/). We are very grateful to the three anonymous reviewers and the editor, whose comments greatly improved the quality of this manuscript.

References

Baker, A. J., and Coauthors, 2019: Enhanced Climate Change Response of Wintertime North Atlantic Circulation, Cyclonic Activity, and Precipitation in a 25-km-Resolution Global Atmospheric Model. *Journal of Climate*, **32 (22)**, 7763–7781, https://doi.org/10.1175/JCLI-D-19-0054.1.

Bals-Elsholz, T. M., E. H. Atallah, L. F. Bosart, T. A. Wasula, M. J. Cempa, and A. R. Lupo, 2001: The Wintertime Southern Hemisphere Split Jet: Structure, Variability, and Evolution. *Journal of Climate*, **14 (21)**, 4191–4215, https://doi.org/10.1175/1520-0442(2001)014<4191:TWSHSJ>2.0.CO;2.

Bock, L., and Coauthors, 2020: Quantifying Progress Across Different CMIP Phases With the ESMValTool. *Journal of Geophysical Research: Atmospheres*, **125 (21)**, e2019JD032 321, https://doi.org/https://doi.org/10.1029/2019JD032321.

Bodas-Salcedo, A., and Coauthors, 2014: Origins of the Solar Radiation Biases over the Southern Ocean in CFMIP2 Models*. *Journal of Climate*, **27 (1)**, 41–56, https://doi.org/10.1175/JCLI-D-13-00169.1.

Bracegirdle, T. J., C. R. Holmes, J. S. Hosking, G. J. Marshall, M. Osman, M. Patterson, and T. Rackow, 2020: Improvements in Circumpolar Southern Hemisphere Extratropical Atmospheric Circulation in CMIP6 Compared to CMIP5. *Earth and Space Science*, **7 (6)**, e2019EA001 065, https://doi.org/https://doi.org/10.1029/2019EA001065.

Bracegirdle, T. J., E. Shuckburgh, J.-B. Sallee, Z. Wang, A. J. S. Meijers, N. Bruneau, T. Phillips, and L. J. Wilcox, 2013: Assessment of surface winds over the Atlantic, Indian, and Pacific Ocean sectors of the Southern Ocean in CMIP5 models: historical bias, forcing response, and state dependence. *Journal of Geophysical Research: Atmospheres*, **118 (2)**, 547–562, https://doi.org/https://doi.org/10.1002/jgrd.50153.

Ceppi, P., Y.-T. Hwang, D. M. W. Frierson, and D. L. Hartmann, 2012: Southern Hemisphere jet latitude biases in CMIP5 models linked to shortwave cloud forcing. *Geophysical Research Letters*, **39 (19)**, https://doi.org/10.1029/2012GL053115.

Chang, E. K. M., Y. Guo, and X. Xia, 2012: CMIP5 multimodel ensemble projection of storm track change under global warming. *Journal of Geophysical Research: Atmospheres*, **117 (D23)**, https://doi.org/10.1029/2012JD018578.

Chang, E. K. M., Y. Guo, X. Xia, and M. Zheng, 2013: Storm-Track Activity in IPCC AR4/CMIP3 Model Simulations. *Journal of Climate*, **26 (1)**, 246–260, https://doi.org/10.1175/JCLI-D-11-00707.1.

Clark, P. A., and S. L. Gray, 2018: Sting jets in extratropical cyclones: a review. *Quarterly Journal of the Royal Meteorological Society*, **144 (713)**, 943–969, https://doi.org/https://doi.org/10.1002/qj.3267.

Curtis, P. E., P. Ceppi, and G. Zappa, 2020: Role of the mean state for the Southern Hemispheric jet stream response to CO2 forcing in CMIP6 models. *Environmental Research Letters*, **15 (6)**, https://doi.org/10.1088/1748-9326/ab8331.

Davini, P., F. Fabiano, and I. Sandu, 2021: Orographic resolution driving the improvements associated with horizontal resolution increase in the Northern Hemisphere winter mid-latitudes. *Weather and Climate Dynamics Discussions*, 1–25, https://doi.org/10.5194/wcd-2021-51.

Dowdy, A. J., and J. L. Catto, 2017: Extreme weather caused by concurrent cyclone, front and thunderstorm occurrences. *Scientific Reports*, **7**, https://doi.org/10.1038/srep40359.

Eyring, V., S. Bony, G. A. Meehl, C. A. Senior, B. Stevens, R. J. Stouffer, and K. E. Taylor, 2016: Overview of the Coupled Model Intercomparison Project Phase 6 (CMIP6) experimental design and organization. *Geoscientific Model Development*, **9 (5)**, 1937–1958, https://doi.org/10.5194/gmd-9-1937-2016.

Flato, G., and Coauthors, 2013: *Evaluation of Climate Models*, book section 2, 741–866. Cambridge University Press, Cambridge, United Kingdom and New York, NY, USA, https://doi.org/10.1017/CBO9781107415324.020, URL www.climatechange2013.org.

Garfinkel, C. I., I. White, E. P. Gerber, and M. Jucker, 2020: The Impact of SST Biases in the Tropical East Pacific and Agulhas Current Region on Atmospheric Stationary Waves in the Southern Hemisphere. *Journal of Climate*, **33 (21)**, 9351–9374, https://doi.org/10.1175/JCLI-D-20-0195.1.

Gates, W. L., and Coauthors, 1999: An Overview of the Results of the Atmospheric Model Intercomparison Project (AMIP I). *Bulletin of the American Meteorological Society*, **80 (1)**, 29–56, https://doi.org/10.1175/1520-0477(1999)080<0029:AOOTRO>2.0.CO;2.

Gelaro, R., and Coauthors, 2017: The Modern-Era Retrospective Analysis for Research and Applications, Version 2 (MERRA-2). *Journal of Climate*, **30 (14)**, 5419–5454, https://doi.org/10.1175/JCLI-D-16-0758.1.

Govekar, P. D., C. Jakob, and J. Catto, 2014: The relationship between clouds and dynamics in Southern Hemisphere extratropical cyclones in the real world and a climate model. *Journal of Geophysical Research: Atmospheres*, **119 (11)**, https://doi.org/10.1002/2013JD020699.

Graff, L. S., and J. H. LaCasce, 2014: Changes in Cyclone Characteristics in Response to Modified SSTs. *Journal of Climate*, **27 (11)**, 4273–4295, https://doi.org/10.1175/JCLI-D-13-00353.1.

Grise, K. M., and M. K. Kelleher, 2021: Midlatitude Cloud Radiative Effect Sensitivity to Cloud Controlling Factors in Observations and Models: Relationship with Southern Hemisphere Jet Shifts and Climate Sensitivity. *Journal of Climate*, **34**, 5869–5886, https://doi.org/10.1175/JCLI-D-20-0986.1.

Grise, K. M., and L. M. Polvani, 2014: Southern Hemisphere Cloud–Dynamics Biases in CMIP5 Models and Their Implications for Climate Projections. *Journal of Climate*, **27 (15)**, 6074–6092, https://doi.org/10.1175/JCLI-D-14-00113.1.

Grose, M. R., J. S. Risbey, A. F. Moise, S. Osbrough, C. Heady, L. Wilson, and T. Erwin, 2016: Constraints on Southern Australian Rainfall Change Based on Atmospheric Circulation in CMIP5 Simulations. *Journal of Climate*, **30 (1)**, 225–242, https://doi.org/10.1175/JCLI-D-16-0142.1.

Gutjahr, O., D. Putrasahan, K. Lohmann, J. H. Jungclaus, J.-S. von Storch, N. Brüggemann, H. Haak, and A. Stössel, 2019: Max Planck Institute Earth System Model (MPI-ESM1.2) for the High-Resolution Model Intercomparison Project (HighResMIP). *Geoscientific Model Development*, **12 (7)**, 3241–3281, https://doi.org/10.5194/gmd-12-3241-2019.

Haarsma, R. J., and Coauthors, 2016: High Resolution Model Intercomparison Project (HighResMIP v1.0) for CMIP6. *Geoscientific Model Development*, **9 (11)**, 4185–4208, https://doi.org/10.5194/gmd-9-4185-2016.

Hawcroft, M. K., L. C. Shaffrey, K. I. Hodges, and H. F. Dacre, 2012: How much Northern Hemisphere precipitation is associated with extratropical cyclones? *Geophysical Research Letters*, **39 (24)**, https://doi.org/10.1029/2012GL053866.

Hersbach, H., and Coauthors, 2020: The ERA5 global reanalysis. *Quarterly Journal of the Royal Meteorological Society*, **146 (730)**, 1999–2049, https://doi.org/10.1002/qj.3803.

Hodges, K. I., 1995: Feature Tracking on the Unit Sphere. *Monthly Weather Review*, **123 (12)**, 3458–3465, https://doi.org/10.1175/1520-0493(1995)123<3458:FTOTUS>2.0.CO;2.

Hodges, K. I., 1996: Spherical Nonparametric Estimators Applied to the UGAMP Model Integration for AMIP. *Monthly Weather Review*, **124 (12)**, 2914–2932, https://doi.org/10.1175/1520-0493(1996)124<2914:SNEATT>2.0.CO;2.

Hodges, K. I., 1999: Adaptive Constraints for Feature Tracking. *Monthly Weather Review*, **127 (6)**, 1362–1373, https://doi.org/10.1175/1520-0493(1999)127<1362:ACFFT>2.0.CO;2.

Hodges, K. I., R. W. Lee, and L. Bengtsson, 2011: A Comparison of Extratropical Cyclones in Recent Reanalyses ERA-Interim, NASA MERRA, NCEP CFSR, and JRA-25. *Journal of Climate*, **24 (18)**, 4888–4906, https://doi.org/10.1175/2011JCLI4097.1.

Hyder, P., and Coauthors, 2018: Critical Southern Ocean climate model biases traced to atmospheric model cloud errors. *Nature Communications*, **9 (1)**, 3625.

Inatsu, M., and B. J. Hoskins, 2004: The Zonal Asymmetry of the Southern Hemisphere Winter Storm Track. *Journal of Climate*, **17 (24)**, 4882–4892, https://doi.org/10.1175/JCLI-3232.1.

Inatsu, M., and B. J. Hoskins, 2006: The Seasonal and Wintertime Variability of the Split Jet and the Storm-Track Activity Minimum Near New Zealand. *J. Meteor. Soc. Japan*, **84 (3)**, 433–445, https://doi.org/https://doi.org/10.2151/jmsj.84.433.

James, I. N., 1988: On the forcing of planetary-scale Rossby waves by Antarctica. *Quarterly Journal of the Royal Meteorological Society*, **114 (481)**, 619–637, https://doi.org/10.1002/qj.49711448105.

Kajtar, J. B., A. Santoso, M. Collins, A. S. Taschetto, M. H. England, and L. M. Frankcombe, 2021: CMIP5 Intermodel Relationships in the Baseline Southern Ocean Climate System and

With Future Projections. *Earth's Future*, **9 (6)**, e2020EF001 873, https://doi.org/https://doi.org/10.1029/2020EF001873.

Kaspi, Y., and T. Schneider, 2013: The Role of Stationary Eddies in Shaping Midlatitude Storm Tracks. *Journal of the Atmospheric Sciences*, **70 (8)**, 2596–2613, https://doi.org/10.1175/JAS-D-12-082.1.

Kawai, H., S. Yukimoto, T. Koshiro, N. Oshima, T. Tanaka, H. Yoshimura, and R. Nagasawa, 2019: Significant improvement of cloud representation in the global climate model mri-esm2. *Geoscientific Model Development*, **12 (7)**, 2875–2897, https://doi.org/10.5194/gmd-12-2875-2019, URL https://www.geosci-model-dev.net/12/2875/2019/.

Kidston, J., and E. P. Gerber, 2010: Intermodel variability of the poleward shift of the austral jet stream in the CMIP3 integrations linked to biases in 20th century climatology. *Geophysical Research Letters*, **37 (9)**, https://doi.org/10.1029/2010GL042873.

Kobayashi, S., and Coauthors, 2015: The JRA-55 Reanalysis: General Specifications and Basic Characteristics. *Journal of the Meteorological Society of Japan*, **93 (1)**, 5–48, https://doi.org/10.2151/jmsj.2015-001.

Lee, R. W., 2015: Storm track biases and changes in a warming climate from an extratropical cyclone perspective using CMIP5. Ph.D. thesis, University of Reading.

Li, Y., D. W. J. Thompson, and S. Bony, 2015: The Influence of Atmospheric Cloud Radiative Effects on the Large-Scale Atmospheric Circulation. *Journal of Climate*, **28 (18)**, 7263–7278, https://doi.org/10.1175/JCLI-D-14-00825.1.

Lindsay, R., M. Wensnahan, A. Schweiger, and J. Zhang, 2014: Evaluation of Seven Different Atmospheric Reanalysis Products in the Arctic. *Journal of Climate*, **27 (7)**, 2588–2606, https://doi.org/10.1175/JCLI-D-13-00014.1.

Loeb, N. G., and Coauthors, 2018: Clouds and the Earth's Radiant Energy System (CERES) Energy Balanced and Filled (EBAF) Top-of-Atmosphere (TOA) Edition-4.0 Data Product. *Journal of Climate*, **31 (2)**, 895–918, https://doi.org/10.1175/JCLI-D-17-0208.1.

Mauritsen, T., and Coauthors, 2019: Developments in the MPI-M Earth System Model version 1.2 (MPI-ESM1.2) and Its Response to Increasing CO2. *Journal of Advances in Modeling Earth Systems*, **11 (4)**, 998–1038, https://doi.org/10.1029/2018MS001400.

Meehl, G. A., C. Covey, T. Delworth, M. Latif, B. McAvaney, J. F. B. Mitchell, R. J. Stouffer, and K. E. Taylor, 2007: The WCRP CMIP3 Multimodel Dataset: A New Era in Climate Change Research. *Bulletin of the American Meteorological Society*, **88 (9)**, 1383 – 1394, https://doi.org/10.1175/BAMS-88-9-1383.

Menary, M. B., D. L. R. Hodson, J. I. Robson, R. T. Sutton, R. A. Wood, and J. A. Hunt, 2015: Exploring the impact of CMIP5 model biases on the simulation of North Atlantic decadal variability. *Geophysical Research Letters*, **42 (14)**, 5926–5934, https://doi.org/https://doi.org/10.1002/2015GL064360.

Met Office, 2010 - 2013: *Iris: A Python library for analysing and visualising meteorological and oceanographic data sets*. Exeter, Devon, v1.2 ed., URL http://scitools.org.uk/.

Mooney, P. A., F. J. Mulligan, and R. Fealy, 2011: Comparison of ERA-40, ERA-Interim and NCEP/NCAR reanalysis data with observed surface air temperatures over Ireland. *International Journal of Climatology*, **31 (4)**, 545–557, https://doi.org/10.1002/joc.2098.

Nakamura, H., T. Sampe, A. Goto, W. Ohfuchi, and S.-P. Xie, 2008: On the importance of midlatitude oceanic frontal zones for the mean state and dominant variability in the tropospheric circulation. *Geophysical Research Letters*, **35 (15)**, https://doi.org/10.1029/2008GL034010.

Nakayama, M., H. Nakamura, and F. Ogawa, 2021: Impacts of a Midlatitude Oceanic Frontal Zone for the Baroclinic Annular Mode in the Southern Hemisphere. *Journal of Climate*, https://doi.org/10.1175/JCLI-D-20-0359.1.

Nie, Y., Y. Zhang, X.-Q. Yang, and H.-L. Ren, 2019: Winter and Summer Rossby Wave Sources in the CMIP5 Models. *Earth and Space Science*, **6 (10)**, 1831–1846, https://doi.org/https://doi.org/10.1029/2019EA000674.

Patterson, M., T. Bracegirdle, and T. Woollings, 2019: Southern Hemisphere Atmospheric Blocking in CMIP5 and Future Changes in the Australia-New Zealand Sector. *Geophysical Research Letters*, **0 (0)**, https://doi.org/10.1029/2019GL083264.

Patterson, M., T. Woollings, T. Bracegirdle, and N. T. Lewis, 2020: Wintertime Southern Hemisphere jet streams shaped by interaction of transient eddies with Antarctic orography. *Journal of Climate*, 1–57, https://doi.org/10.1175/JCLI-D-20-0153.1.

Pithan, F., T. G. Shepherd, G. Zappa, and I. Sandu, 2016: Climate model biases in jet streams, blocking and storm tracks resulting from missing orographic drag. *Geophysical Research Letters*, **43 (13)**, 7231–7240, https://doi.org/10.1002/2016GL069551.

Priestley, M. D. K., D. Ackerley, J. L. Catto, and K. I. Hodges, 2022: Drivers of biases in the CMIP6 extratropical storm tracks. Part 1: Northern Hemisphere. *Journal of Climate*, 1–37, https://doi.org/10.1175/JCLI-D-20-0976.1.

Priestley, M. D. K., D. Ackerley, J. L. Catto, K. I. Hodges, R. E. McDonald, and R. W. Lee, 2020: An Overview of the Extratropical Storm Tracks in CMIP6 Historical Simulations. *Journal of Climate*, **33 (15)**, 6315–6343, https://doi.org/10.1175/JCLI-D-19-0928.1.

Roberts, M. J., and Coauthors, 2019: Description of the resolution hierarchy of the global coupled HadGEM3-GC3.1 model as used in CMIP6 HighResMIP experiments. *Geoscientific Model Development*, **12 (12)**, 4999–5028, https://doi.org/10.5194/gmd-12-4999-2019.

Sallée, J.-B., E. Shuckburgh, N. Bruneau, A. J. S. Meijers, T. J. Bracegirdle, Z. Wang, and T. Roy, 2013: Assessment of Southern Ocean water mass circulation and characteristics in CMIP5 models: Historical bias and forcing response. *Journal of Geophysical Research: Oceans*, **118 (4)**, 1830–1844, https://doi.org/10.1002/jgrc.20135.

Sandu, I., and Coauthors, 2019: Impacts of orography on large-scale atmospheric circulation. *npj Climate and Atmospheric Science*, **2 (1)**, 10.

Stouffer, R. J., V. Eyring, G. A. Meehl, S. Bony, C. Senior, B. Stevens, and K. E. Taylor, 2017: CMIP5 Scientific Gaps and Recommendations for CMIP6. *Bulletin of the American Meteorological Society*, **98 (1)**, 95–105, https://doi.org/10.1175/BAMS-D-15-00013.1.

Tamarin, T., and Y. Kaspi, 2016: The Poleward Motion of Extratropical Cyclones from a Potential Vorticity Tendency Analysis. *Journal of the Atmospheric Sciences*, **73 (4)**, 1687–1707, https://doi.org/10.1175/JAS-D-15-0168.1.

Taylor, K. E., R. J. Stouffer, and G. A. Meehl, 2012: An Overview of CMIP5 and the Experiment Design. *Bulletin of the American Meteorological Society*, **93 (4)**, 485–498, https://doi.org/10.1175/BAMS-D-11-00094.1.

Taylor, K. E., and Coauthors, 2017: CMIP6 Global Attributes, DRS, Filenames, Directory Structure and, CV's. Tech. Rep. v6.2.6, Program for Climate Model Diagnosis and Intercomparison, http://goo.gl/v1drZl.

Tian, B., and X. Dong, 2020: The Double-ITCZ Bias in CMIP3, CMIP5, and CMIP6 Models Based on Annual Mean Precipitation. *Geophysical Research Letters*, **47 (8)**, e2020GL087 232, https://doi.org/10.1029/2020GL087232.

Trenberth, K. E., and J. T. Fasullo, 2010: Simulation of Present-Day and Twenty-First-Century Energy Budgets of the Southern Oceans. *Journal of Climate*, **23 (2)**, 440–454, https://doi.org/10.1175/2009JCLI3152.1.

Trenberth, K. E., J. T. Fasullo, and J. Mackaro, 2011: Atmospheric Moisture Transports from Ocean to Land and Global Energy Flows in Reanalyses. *Journal of Climate*, **24 (18)**, 4907–4924, https://doi.org/10.1175/2011JCLI4171.1.

Tsujino, H., and Coauthors, 2020: Evaluation of global ocean–sea-ice model simulations based on the experimental protocols of the Ocean Model Intercomparison Project phase 2 (OMIP-2). *Geoscientific Model Development*, **13 (8)**, 3643–3708, https://doi.org/10.5194/gmd-13-3643-2020.

Voigt, A., and T. A. Shaw, 2015: Circulation response to warming shaped by radiative changes of clouds and water vapour. *Nature Geoscience*, **8**, 102–106, https://doi.org/10.1038/ngeo2345.

Wang, C., L. Zhang, S.-K. Lee, L. Wu, and C. R. Mechoso, 2014: A global perspective on CMIP5 climate model biases. *Nature Climate Change*, **4 (3)**, 201–205, https://doi.org/10.1038/nclimate2118.

Wilcox, L. J., A. J. Charlton-Perez, and L. J. Gray, 2012: Trends in Austral jet position in ensembles of high- and low-top CMIP5 models. *Journal of Geophysical Research: Atmospheres*, **117 (D13)**, https://doi.org/10.1029/2012JD017597.

Williams, K. D., and A. Bodas-Salcedo, 2017: A multi-diagnostic approach to cloud evaluation. *Geoscientific Model Development*, **10 (7)**, 2547–2566, https://doi.org/10.5194/gmd-10-2547-2017.

Williams, K. D., and Coauthors, 2013: The Transpose-AMIP II Experiment and Its Application to the Understanding of Southern Ocean Cloud Biases in Climate Models. *Journal of Climate*, **26 (10)**, 3258–3274, https://doi.org/10.1175/JCLI-D-12-00429.1.

Willison, J., W. A. Robinson, and G. M. Lackmann, 2013: The Importance of Resolving Mesoscale Latent Heating in the North Atlantic Storm Track. *Journal of the Atmospheric Sciences*, **70 (7)**, 2234–2250, https://doi.org/10.1175/JAS-D-12-0226.1.

Wood, T., C. M. McKenna, A. Chrysanthou, and A. C. Maycock, 2020: Role of sea surface temperature patterns for the Southern Hemisphere jet stream response to CO2 forcing. *Environmental Research Letters*, **16 (1)**, 014 020, https://doi.org/10.1088/1748-9326/abce27.

Zelinka, M. D., T. A. Myers, D. T. McCoy, S. Po-Chedley, P. M. Caldwell, P. Ceppi, S. A. Klein, and K. E. Taylor, 2020: Causes of Higher Climate Sensitivity in CMIP6 Models. *Geophysical Research Letters*, **47 (1)**, e2019GL085 782, https://doi.org/10.1029/2019GL085782.